

Microprobing the molecular spatial distribution and structural architecture of feed-type sorghum seed tissue (*Sorghum Bicolor L.*) using the synchrotron radiation infrared microspectroscopy technique

Peiqiang Yu

College of Agriculture and Bioresources, University of Saskatchewan, 51 Campus Drive, Saskatoon, SK, Canada. E-mail: peiqiang.yu@usask.ca

Sorghum seed (*Sorghum bicolor L.*) has unique degradation and fermentation behaviours compared with other cereal grains such as wheat, barley and corn. This may be related to its cell and cell-wall architecture. The advanced synchrotron radiation infrared microspectroscopy (SR-IMS) technique enables the study of cell or living cell biochemistry within cellular dimensions. The objective of this study was to use the SR-IMS imaging technique to microprobe molecular spatial distribution and cell architecture of the sorghum seed tissue comprehensively. High-density mapping was carried out using SR-IMS on beamline U2B at the National Synchrotron Light Source (Brookhaven National Laboratory, NY, USA). Molecular images were systematically recorded from the outside to the inside of the seed tissue under various chemical functional groups and their ratios [peaks at ~ 1725 (carbonyl C=O ester), 1650 (amide I), 1657 (protein secondary structure α -helix), 1628 (protein secondary structure β -sheet), 1550 (amide II), 1515 (aromatic compounds of lignin), 1428, 1371, 1245 (cellulosic compounds in plant seed tissue), 1025 (non-structural CHO, starch granules), 1246 (cellulosic material), 1160 (CHO), 1150 (CHO), 1080 (CHO), 930 (CHO), 860 (CHO), 3350 (OH and NH stretching), 2960 (CH_3 anti-symmetric), 2929 (CH_2 anti-symmetric), 2877 (CH_3 symmetric) and 2848 cm^{-1} (CH_2 asymmetric)]. The relative protein secondary structure α -helix to β -sheet ratio image, protein amide I to starch granule ratio image, and anti-symmetric CH_3 to CH_2 ratio image were also investigated within the intact sorghum seed tissue. The results showed unique cell architecture, and the molecular spatial distribution and intensity in the sorghum seed tissue (which were analyzed through microprobe molecular imaging) were generated using SR-IMS. This imaging technique and methodology has high potential and could be used for scientists to develop specific cereal grain varieties with targeted food and feed quality, and can also be used to monitor the degree of grain maturity, grain damage, the fate of organic contaminants and the effect of chemical treatment on plant and grain seeds.

1. Introduction

Sorghum seed (*Sorghum bicolor L.*) has unique degradation and fermentation behaviours compared with other cereal grain such as wheat, corn and barley. It is expected that the unique degradation and fermentation behaviours are related to the structure and cell-wall architecture of the seeds. Electron microscopy and fluorescence microscopy could be used to look at a visible image of the inherent structure of the tissue. Complementary to these approaches is vibrational molecular

spectroscopy, which could provide chemical information about the sample based on its molecular vibrations (Dokken *et al.*, 2007; Chan *et al.*, 2008).

Attenuated total reflectance (ATR) and polarized infrared spectroscopies in combination with infrared microspectroscopy (IMS) makes sampling rapid and easy, providing direct analysis *in situ* (Dokken *et al.*, 2007). However, conventional global-source IMS is not able to explore the tissue structure within cellular and subcellular dimensions and cannot be used to detect cell architecture. When synchrotron light combines

with IMS it is known as synchrotron radiation infrared microspectroscopy (SR-IMS) (CLS, 2010). Vibrational IMS with synchrotron light can be used for structural and molecular characterization as a rapid and non-destructive technique (Burattini *et al.*, 2008). This technique has emerged as a key technique for studying tissue cell-wall components (McCann & Roberts, 1994; McCann *et al.*, 1995, 1997; Wetzel *et al.*, 1998; Yu *et al.*, 2004; Dokken *et al.*, 2007), for studying plant growth and development (Dokken *et al.*, 2007; McCann & Roberts, 1994; McCann *et al.*, 1995, 1997), monitoring the fate of organic contaminants in plants (Dokken *et al.*, 2005) and studying the bread-making quality of wheat (Bonwell *et al.*, 2008).

Dokken (2006) indicated that current wet chemistry techniques, although helpful, degrade plant tissue resulting in the loss of spatial distribution and the production of artifacts because wet chemistry techniques employ strong chemical processing and extractions such as GC-MS (gas chromatography mass spectrometry) and HPLC (high-performance liquid chromatography). SR-IMS permits direct analysis of plant cell-wall architecture, combining spatially localized information and chemical information from the infrared absorbance to produce a chemical map that can be linked to a particular morphology or functional group (Budevskaa, 2002; Dokken, 2006; Dokken *et al.*, 2007). Dokken (2006) showed that SR-IMS, as an important analytical tool, could be used to determine the fate and effect of organic contaminants in plants.

To our knowledge, SR-IMS has not yet been applied to study structural and molecular characterization and relationship between structure and biological functionality in the feed-type sorghum seed tissue. The objective of this study was to use the advanced synchrotron-based technique SR-IMS to microprobe molecular spatial distribution and structural architecture of the feed-type sorghum seed tissue (*Sorghum bicolor L.*).

2. Materials and methods

2.1. Tissue preparation, photomicrograph and synchrotron-based BaF₂ window preparation

Feed-type sorghum seed (*Sorghum bicolor L.* feed-type) was obtained from Professor Dr D. Liu (Northeast Agriculture University, China). Detailed studies of the sorghum seeds in terms of nutrient characterization, *in situ* degradation kinetics, energy values and nutrient supply have been carried out. The sorghum seeds were cut into thin cross sections (6 μm thickness) using a microtome at The Western College of Veterinary Medicine, University of Saskatchewan (Saskatoon, Canada), and then unstained cross sections were transferred to BaF₂ windows (size: 13 \times 1 mm disc; Spectral Systems, NY, USA) for transmission-mode synchrotron IR microspectroscopic work. Photomicrographs of the cross section of the sorghum seed tissue were recorded using a microscope linked to a digital camera from the BaF₂ window at the U2B station at the

National Synchrotron Light Source (NSLS), Brookhaven National Laboratory (BNL), NY, USA (Fig. 1).

2.2. Synchrotron light source and synchrotron FTIR microspectroscopy at NSLS-BNL

The experiment was carried out on beamline U2B (The Center for Synchrotron Biosciences, Case Western Reserve University) at the National Synchrotron Light Source located in Brookhaven National Laboratory (NSLS-BNL, US Department of Energy, New York). The detailed methodology has been described previously by Yu *et al.* (2004). The beamline is equipped with a FTIR spectrometer (Nicolet Magna 860) with KBr beam-splitter and a mercury cadmium telluride detector coupled to an infrared microscope (Nic Plan, Nicolet Instruments, Madison, WI, USA). The bench was configured to use collimated synchrotron light (beam energy 800 MeV) through an external input on the spectrometer. The modulated light was passed through the Nic Plan IR microscope and used to perform transmission microscopy. Infrared spectra were collected in the mid-IR range, 4000–800 cm^{-1} , at a resolution of 4 cm^{-1} with 64 scans co-added and an aperture setting of $\sim 10 \mu\text{m} \times 10 \mu\text{m}$. To minimize infrared absorption by CO₂ and water vapour in the ambient air, the optics were purged using dry N₂. A background spectrum was collected from an area free of sample. Mapping steps were equal to the aperture size. Stage control, data collection and processing were performed using *OMNIC 7.2* software (Thermo-Nicolet, Madison, WI, USA). Scanned visible images were obtained using a CCD camera linked to the infrared images (objective $\times 32$).

2.3. Molecular spectral data analysis and imaging molecular chemistry in complex plant system

The spectral data of the tissues were collected and analyzed using *OMNIC 7.2* software. The data can be displayed as either a series of spectroscopic images collected at individual wavelengths, or as a collection of infrared spectra obtained at each pixel position in the image, as described previously (Yu *et al.*, 2004; Miller & Dumas, 2006; Dokken *et al.*, 2007; Miller, 2009).

The molecular images were recorded from the outside to the inside of the tissue (Fig. 1) under various chemical functional groups peaks centred at ~ 1725 (carbonyl C=O ester), 1650 (amide I), 1657 (protein secondary structure α -helix), 1628 (protein secondary structure β -sheet), 1550 (amide II), 1515 (aromatic compounds of lignin), 1428, 1371, 1245 (cellulosic compounds), 1025 (non-structural CHO, starch granules), 1550 (amide II), 1246 (cellulosic material), 1160 (CHO), 1150 (CHO), 1080 (CHO), 930 (CHO), 860 (CHO), 3350 (OH and NH stretching), 2960 (CH₃ anti-symmetric), 2929 (CH₂ anti-symmetric), 2877 (CH₃ symmetric) and 2848 cm^{-1} (CH₂ asymmetric) using *OMNIC 7.2* software. The band assignments of the above functional groups were obtained from the literature (Mathlouthi & Koenig, 1986; Kemp, 1991; Stewart *et al.*, 1995; Wetzel *et al.*, 1998, 2003; Himmelsbach *et al.*, 1998; Wetzel, 2001; Martin, 2002; Marin-

kovic *et al.*, 2002; Marinkovic & Chance, 2006). The protein secondary structure (Jackson & Mantsch, 1995, 1996, 2000; Marinkovic & Chance, 2006) α -helix to β -sheet ratio image, the protein amide I to starch granule ratio image, and the anti-symmetric CH₃ to CH₂ ratio image were determined within intact tissue, representing the distribution of the biological component ratio (or nutrient component ratio) of the tissue (Yu *et al.*, 2004). The ratios were obtained by dividing the area or height under one molecular functional group band (*e.g.* amide I, $\sim 1650\text{ cm}^{-1}$) by the area under another molecular functional group band (*e.g.* non-structural CHO, 1025 cm^{-1}) (Wetzel *et al.*, 1998, 2003) at each pixel (pixel size $10\text{ }\mu\text{m} \times 10\text{ }\mu\text{m}$). False-colour maps derived from the area under particular spectral features were used to represent the distribution and intensity of functional groups across the area of interest.

3. Results and discussion

3.1. Current progress of SR-IMS in plant science research

Recently, SR-IMS has emerged as the most powerful tool for structural and functional investigations in biology because of its ability to provide information on processes at multiple levels of organization (LNF, 2003). It has been used to investigate structural–functional relationships and molecular mechanisms at the atomic level (LNF, 2003). SR-IMS, together with non-supervised (hierarchical cluster analysis, principal component analysis) and/or supervised classification (linear discriminant analysis, artificial neural network) techniques (Sockalingum *et al.*, 1998; Burattini *et al.*, 2008) has been applied to discriminate, identify and classify soybean (Pietrzak & Miller, 2005), barley, wheat and corn (Yu *et al.*, 2004, 2007), as well as to characterize structural change relating to various technological (*e.g.* heat processing, bioethanol processing) and biotechnological (*e.g.* gene transformation) processes (Doiron *et al.*, 2009*a,b*; Yu, 2010).

3.2. Tissue photomicrograph of feed-type sorghum seed

The feed-type sorghum seed (*Sorghum bicolor L.*) has unique degradation and fermentation behaviours compared with wheat, corn and barley grains. It is expected that this is highly related to its intrinsic structure. A unique intrinsic structure usually results in a unique molecular infrared spectrum. Mid-infrared spectroscopy measures the contribution of particular organic and inorganic functional groups within molecules from their induced vibrations (Marinkovic *et al.*, 2002; Wetzel, 2001). However, conventional FTIR (with or without ATR) spectroscopy, near-IR spectroscopy and DRIFT spectroscopy could not reveal plant inherent structures within intact tissue as indicated previously (Yu, 2004; Dokken *et al.*, 2007). Normally they require finely ground samples. Global-source FTIR microspectroscopy could not reveal tissue structure within diffraction limits of a few micrometres (within cellular dimensions) and less light overall results in a decrease of the signal-to-noise ratio (Raab & Martin, 2001). Normally plant cell size is on the micrometre

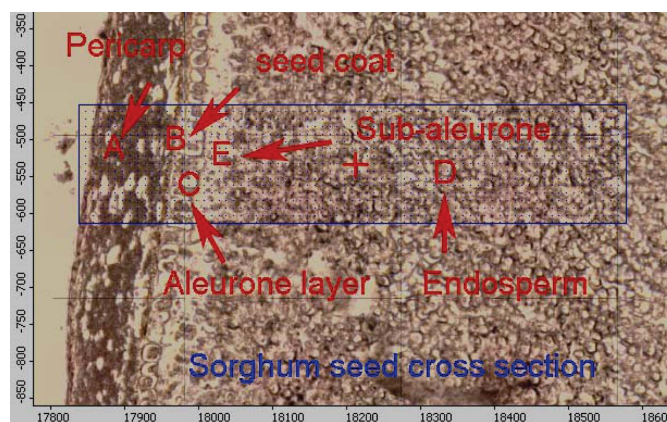


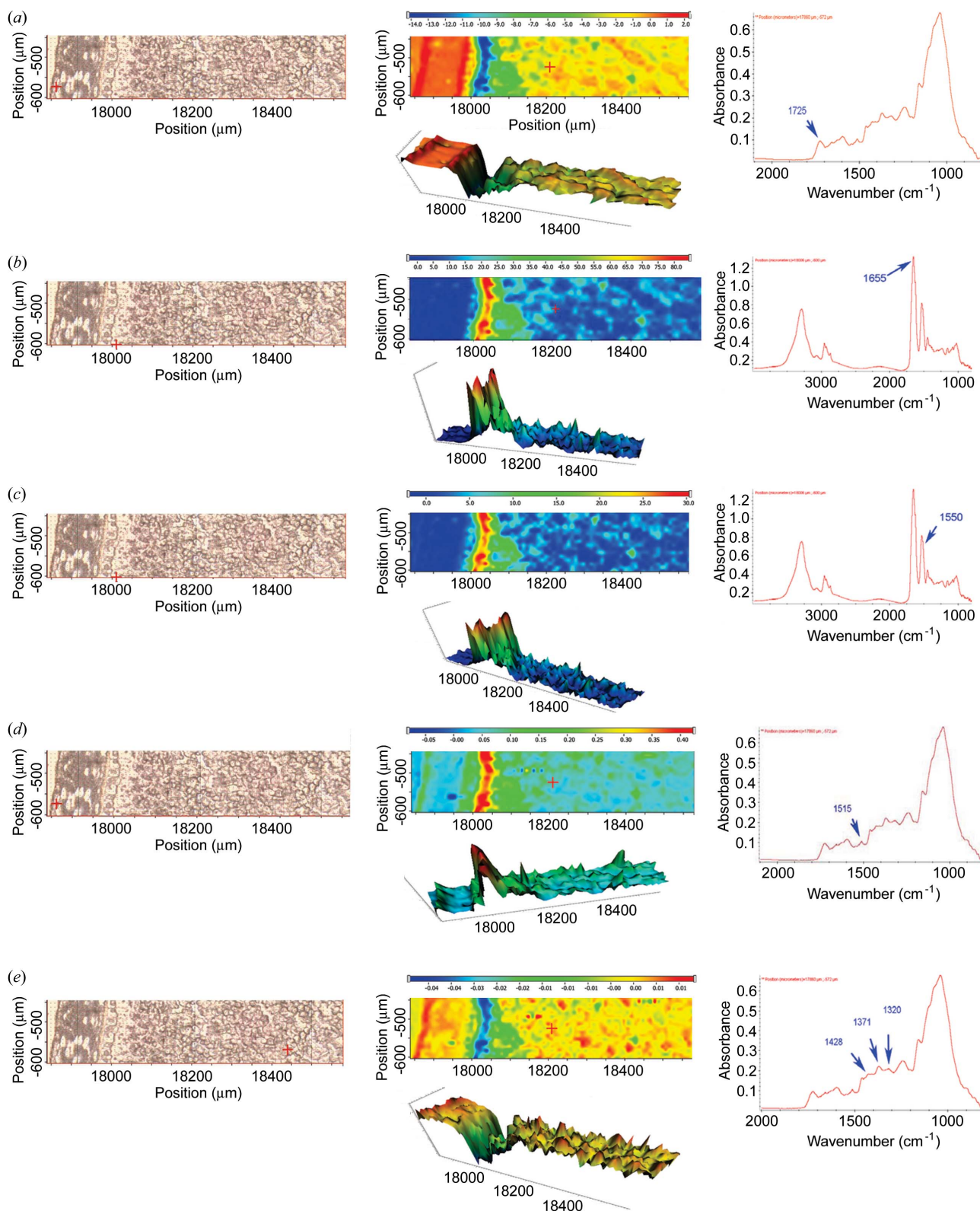
Figure 1

Photomicrograph of the cross section of sorghum ($6\text{ }\mu\text{m}$) showing the intrinsic structure of sorghum from pericarp (A: outside of seed), seed coat (B), aleurone layer (C), endosperm (D) and sub-aleurone endosperm (E).

scale. Electron microscopy can be used to look at plant cells but it only provides a visible image. No chemical image can be produced by electron microscopy (Yu, 2004; Dokken, 2006; Dokken *et al.*, 2007). Fig. 1 presents a photomicrograph of the cross section of a feed-type sorghum seed showing the intrinsic structure of sorghum from the pericarp (A, outside of seed), seed coat (B), aleurone layer (C), endosperm (D) and sub-aleurone endosperm (E). The physiological functions of each layer are different (Yu *et al.*, 2004). With a visible image it is impossible to link structure information to chemical information within cellular dimensions.

3.3. Ultra-spatial distribution of molecular functional groups

SR-IMS, taking advantage of bright synchrotron light (Raab & Martin, 2001), enables detection of molecular chemical features of biological samples at high ultra-spatial resolutions without destructing the inherent structure of the tissue (Wetzel *et al.*, 1998; Yu *et al.*, 2004; Miller & Dumas, 2006; Marinkovic & Chance, 2006; Dokken *et al.*, 2007). Fig. 2 shows colour maps of molecular functional groups from a cross section of the sorghum tissue and single pixel spectra from a sample area of $10\text{ }\mu\text{m} \times 10\text{ }\mu\text{m}$. Molecular functional group images of the feed-type sorghum seed tissue from the pericarp (outside) to seed coat, through the aleurone layer to the endosperm, could be mapped under peaks at ~ 1725 (carbonyl C=O ester), 1650 (protein amide I), 1657 (protein secondary structure α -helix), 1628 (protein secondary structure β -sheet), 1550 (protein amide II), 1515 (aromatic compounds of lignin), 1428 , 1371 , 1245 (cellulosic compounds), 1025 (non-structural CHO, starch granules), 1550 (amide II), 1246 (cellulosic material), 1160 (CHO), 1150 (CHO), 1080 (CHO), 930 (CHO), 860 (CHO), 3350 (OH and NH stretching), 2960 (CH₃ anti-symmetric), 2929 (CH₂ anti-symmetric), 2877 (CH₃ symmetric) and 2848 cm^{-1} (CH₂ asymmetric). The spectral intensities and distributions of various chemical functional groups in feed-type sorghum seed are different from those of corn (Yu *et al.*, 2004) and wheat


Figure 2

Molecular functional group images of the sorghum seed tissue from the pericarp (outside), seed coat, aleurone layer and endosperm [from left to right: visible image; chemical image, peak area of one peak; spectrum corresponding to the pixel at the cross hair in the visible image (spectrum pixel size: $10\ \mu\text{m} \times 10\ \mu\text{m}$)], using synchrotron-based infrared microspectroscopy at the NSLS. (a) Area under the $1725\ \text{cm}^{-1}$ peak (carbonyl $\text{C}=\text{O}$); (b) area under the $1655\ \text{cm}^{-1}$ peak (amide I); (c) area under the $1650\ \text{cm}^{-1}$ peak (amide II); (d) area under the $1515\ \text{cm}^{-1}$ peak (aromatic compound); (e) height under the $1428\ \text{cm}^{-1}$ peak (cellulosic compound); (f) height under the $1371\ \text{cm}^{-1}$ peak (cellulosic compound); (g) area under the $1245\ \text{cm}^{-1}$ peak (cellulosic materials); (h) area under the $1185\text{--}950\ \text{cm}^{-1}$ peak (total CHO); (i) area under the $1160\ \text{cm}^{-1}$ peak (CHO); (j) area under the $1150\ \text{cm}^{-1}$ peak (CHO); (k) area under the $1080\ \text{cm}^{-1}$ peak (CHO); (l) area under the $1025\ \text{cm}^{-1}$ peak (starch); (m) area under the $930\ \text{cm}^{-1}$ peak (CHO); (n) area under the $860\ \text{cm}^{-1}$ peak (CHO); (o) area under the $3350\ \text{cm}^{-1}$ peak (OH and NH: protein and CHO).

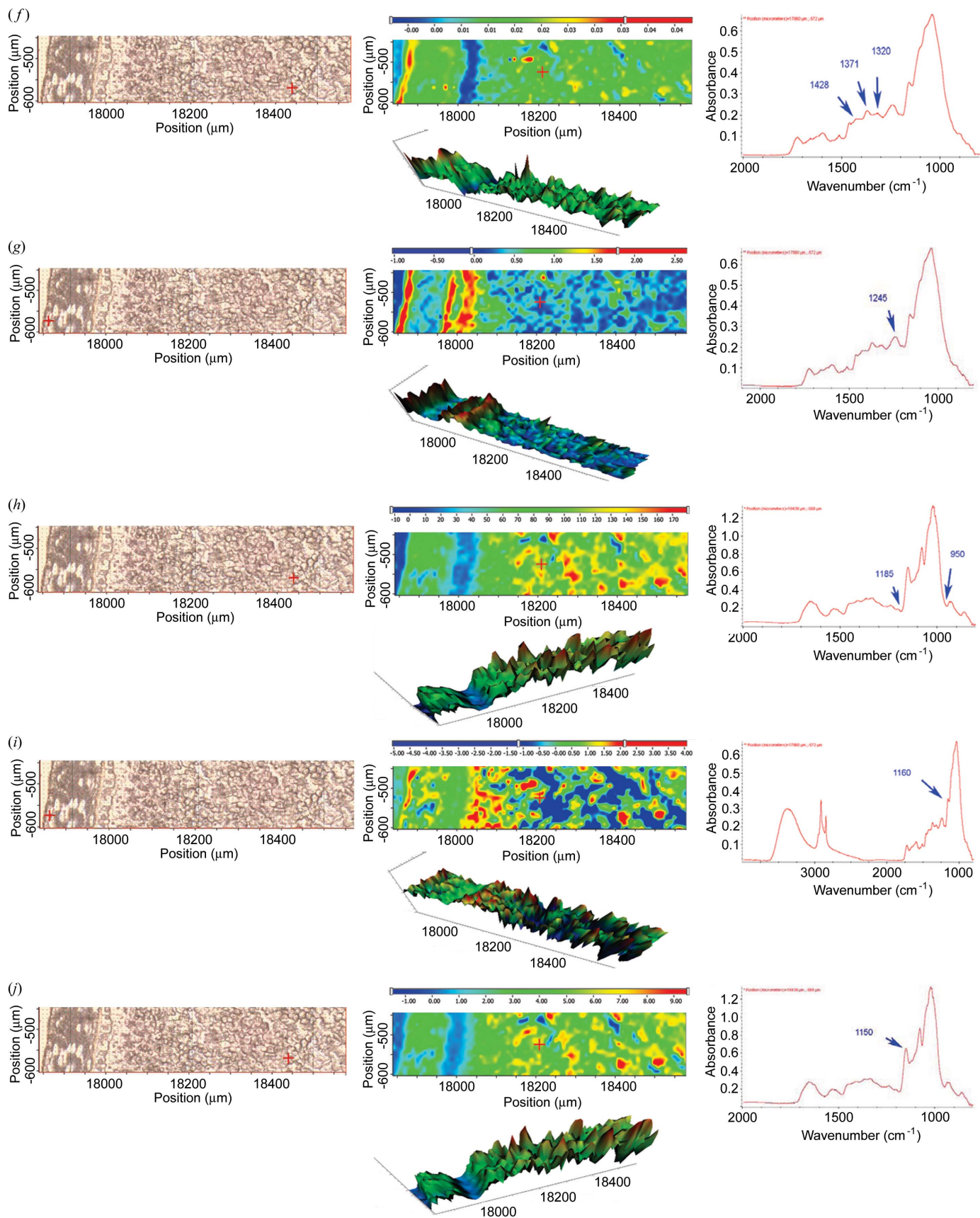


Figure 2 (continued)

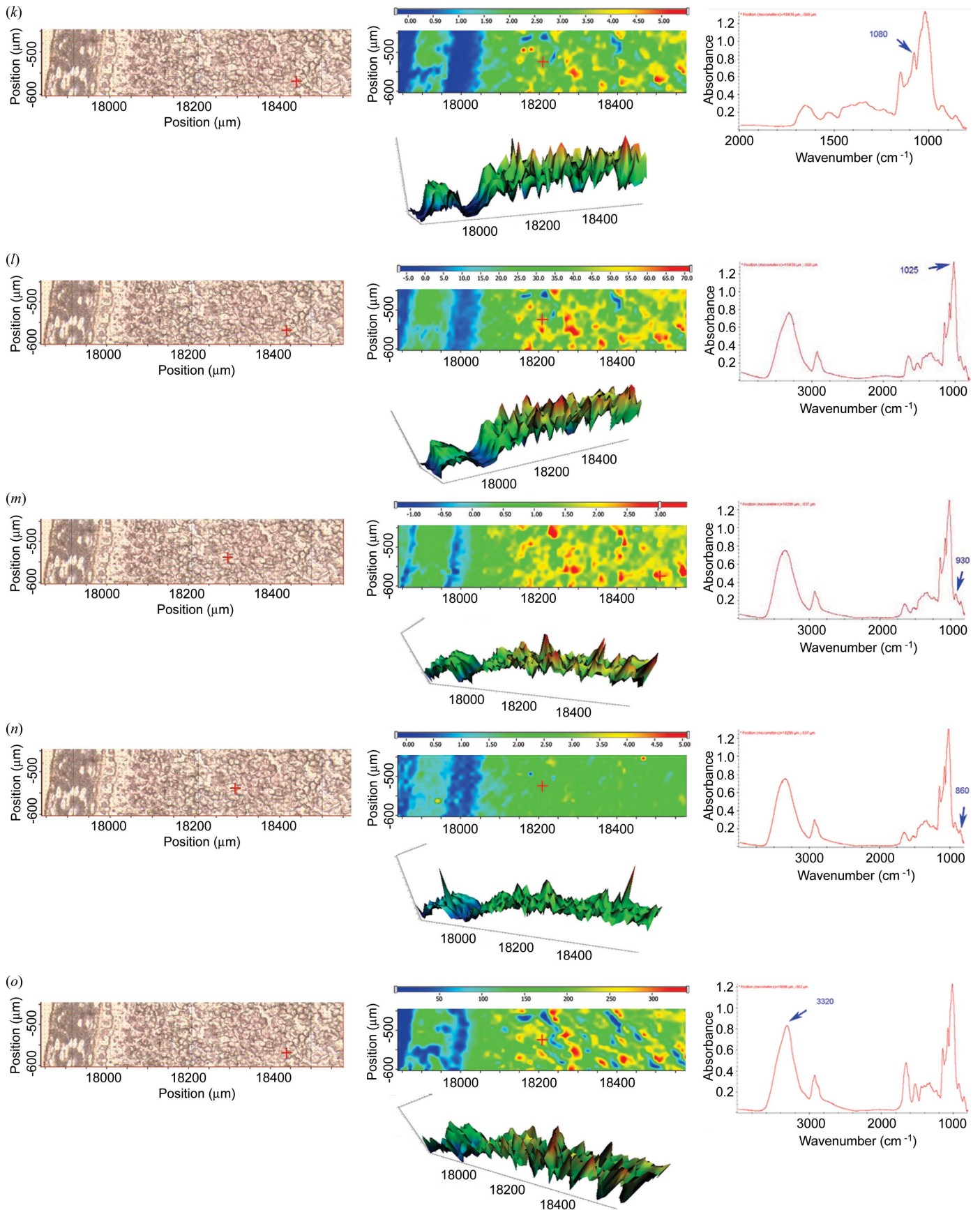


Figure 2 (continued)

(Yu *et al.*, 2007). The molecular functional groups are related to food and feed quality, nutrient availability and functionality. For example, Bonwell *et al.* (2008) indicated that the predominance of α -helix secondary protein structure compared with the β -sheet form is an important molecular structural feature that distinguishes the quality of a wheat cultivar for bread-making.

3.4. Imaging pectin and amides I and II within the intact tissue

SR-IMS is able to show the structural architecture of the feed-type sorghum tissue. Vogel *et al.* (2002) reported that in plant leaves the $\sim 1732\text{ cm}^{-1}$ feature arises from methyl-esterified pectins, not just lipid in cereal grain (Wetzel *et al.*, 1998). Fig. 2(a) shows that the carbonyl C=O ester band ($\sim 1725\text{ cm}^{-1}$) associated with methylesterified pectin is highly concentrated in the pericarp region, followed by the endosperm, sub-aleurone endosperm region, and least concentrated in the aleurone cell layer region. Protein and protein matrix in seed tissue play an important role in nutrient availability and seedling development. Protein shows unique molecular spectra peaks: amide I (1650 cm^{-1}) and amide II (1550 cm^{-1}). Figs. 2(b) and 2(c) show that amides I and II are rich in the aleurone cell layer, followed by the sub-aleurone endosperm region. The other regions, pericarp and endosperm, in the sorghum tissue contain limited amounts of amides I and II. This result indicates that the aleurone cells in seeds are rich in protein content, which may be needed for seedling development (Yu *et al.*, 2004, 2007).

3.5. Imaging aromatic lignin compounds within the intact tissue

Tissue imaging at the $\sim 1515\text{ cm}^{-1}$ peak is shown in Fig. 2(d), indicating the spatial distribution of aromatic lignin compound in the feed-type sorghum tissue. As discussed previously (Himmelsbach *et al.*, 1998; Yu *et al.*, 2004, 2007), the unique absorption band of lignin is found at $\sim 1515\text{ cm}^{-1}$. This is considered to be indicative of the aromatic character of the lignin. An aromatic compound shows two major bands at ~ 1600 and 1515 cm^{-1} , resulting from quadrant and semicircle ring stretching, respectively (Colthup *et al.*, 1990; Himmelsbach *et al.*, 1998). The 1515 cm^{-1} band (Colthup *et al.*, 1990; Wetzel *et al.*, 1998; Himmelsbach *et al.*, 1998) corresponds to the stretch associated with para-substituted benzene rings and can be associated with aromatic species present in the pericarp, seed coat and aleurone layer of the tissue (Yu *et al.*, 2004). However, it should be pointed out that the amide II band may partially interfere with the aromatic ring of lignin in this region. Application of cluster analysis in the chemical image could accurately reveal aromatic lignin features within cellular dimensions (Himmelsbach *et al.*, 1998; Yu, 2005a,b).

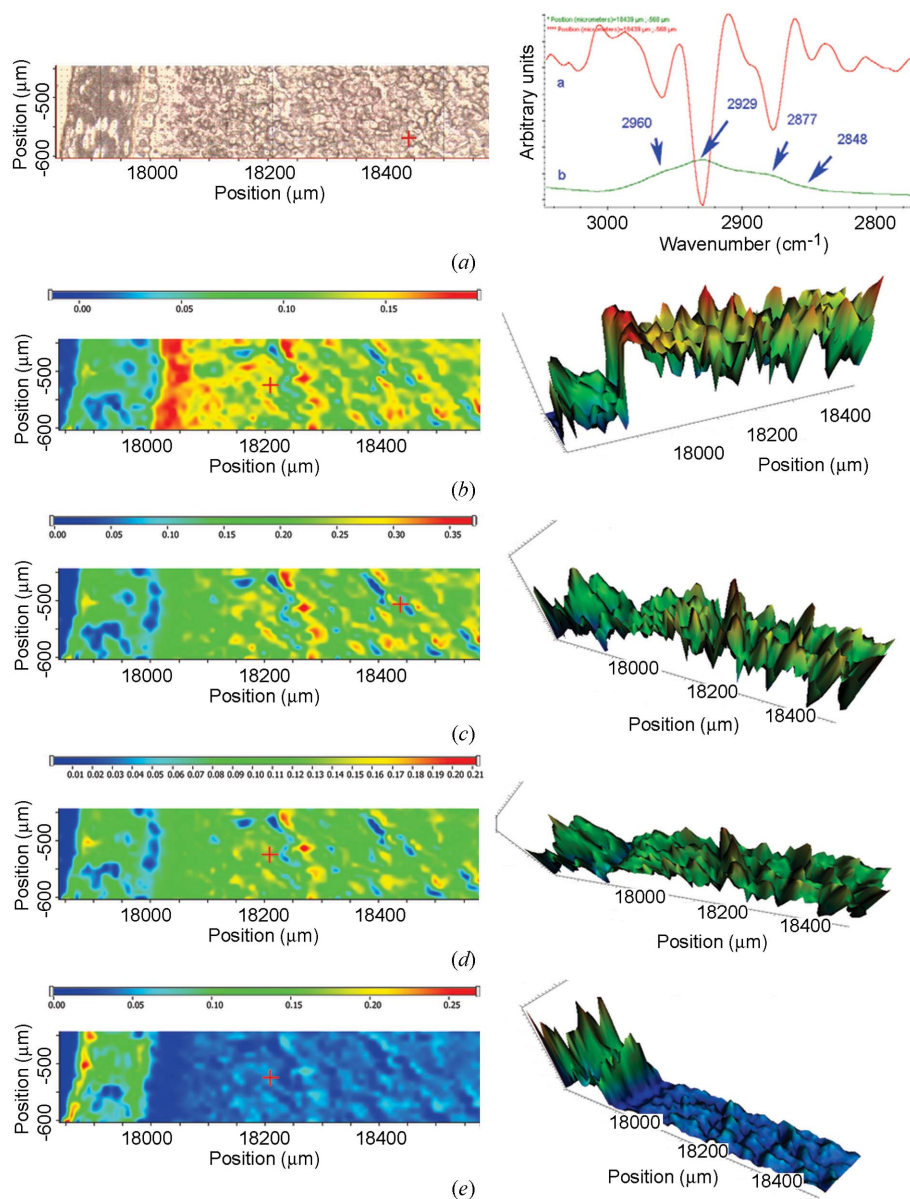
3.6. Imaging cellulosic compounds of structural carbohydrate and starch of non-structural carbohydrate within the intact tissue

In complex plant systems there are two types of carbohydrates: structural and non-structural. In cereal grain non-structural carbohydrates are starch granules; structural carbohydrates are cellulosic and hemicellulosic carbohydrates. In mid-infrared regions, peaks at ~ 1420 , 1370 , 1335 and 1245 cm^{-1} indicate characteristics of structural carbohydrates in cereal grains (Wetzel *et al.*, 1998; Wetzel, 2001). A peak at $\sim 1025\text{ cm}^{-1}$ is indicative of non-structural carbohydrates such as starch in the endosperm of cereal grain (Wetzel *et al.*, 1998; Wetzel, 2001). The major absorption bands from carbohydrates are found in the ~ 1180 – 950 cm^{-1} region of the spectrum (Mathlouthi & Koenig, 1986). Figs. 2(e), 2(f) and 2(g) show chemical images under the area at ~ 1428 , 1371 and 1245 cm^{-1} , revealing the ultra-spatial distribution of cellulosic material and its concentration in the sorghum tissue. The results shows that the pericarp and seed coat contain a relatively high amount of cellulosic materials, but the aleurone layer and endosperm region contain much less structural CHO. Figs. 2(h)–2(n) show various carbohydrate images. The spectra for carbohydrate assignments are very complicated and are not fully understood in complex plant systems in this region. The chemical image under the area at $\sim 1025\text{ cm}^{-1}$ shows that the endosperm region contains a relatively high amount of non-structural CHO. This is due to the large deposition of starch granules in the endosperm regions. Bonwell *et al.* (2008) also report that with the synchrotron technique the microscopic view of wheat endosperm is dominated by many large starch granules with protein in between. The spectrum produced from *in situ* microspectroscopy of this mixture is dominated by carbohydrate bands from the large starch granules that fill up the field (Wetzel *et al.*, 1998; Bonwell *et al.*, 2008).

3.7. Imaging molecular functional group ratios within the intact tissue

The advantage of the functional group ratio image is that it can eliminate the effect of uneven tissue thickness.

3.7.1. Imaging anti-symmetric CH_3 and CH_2 and symmetric CH_3 and CH_2 and their ratio. In the mid-infrared region the dominant absorption features of the lipid spectrum are found in the region 2800 – 3000 cm^{-1} , and were assigned by analogy with the infrared spectra of alkanes. These are predominantly anti-symmetric and symmetric stretching vibrations of the CH_3 (~ 2956 and 2874 cm^{-1}) and CH_2 (~ 2922 and 2852 cm^{-1}) groups of the acyl chains (Miller, 2000; Jackson & Mantsch, 2000; Wetzel & LeVine, 2000; Yu *et al.*, 2004, 2007). In feed-type sorghum seeds the dominant absorption bands for CH_3 anti-symmetric stretching were at $\sim 2960\text{ cm}^{-1}$, CH_2 anti-symmetric stretching at $\sim 2929\text{ cm}^{-1}$, CH_3 symmetric stretching at $\sim 2877\text{ cm}^{-1}$ and CH_2 asymmetric stretching at $\sim 2848\text{ cm}^{-1}$ (Fig. 3). In the Pioneer corn study the centres of the dominant absorption bands for the CH_3 and CH_2 anti-symmetric stretch and CH_3 and CH_2


Figure 3

(a) CH functional group images of the sorghum seed tissue from the pericarp (outside), seed coat, aleurone layer and endosperm. Left: visible image. Right: spectra corresponding to the pixel at the cross hair in the visible image. Spectrum pixel size: $10 \mu\text{m} \times 10 \mu\text{m}$. (b) CH_3 anti-symmetric stretch at $\sim 2960 \text{ cm}^{-1}$; (c) CH_2 anti-symmetric stretch at $\sim 2929 \text{ cm}^{-1}$; (d) CH_3 symmetric stretch at $\sim 2877 \text{ cm}^{-1}$; (e) CH_2 asymmetric stretch at $\sim 2848 \text{ cm}^{-1}$. Left, for (b)–(e): visible image; right: chemical image, peak height of one peak.

symmetric stretch were slightly different from this study with a $\sim \pm 5 \text{ cm}^{-1}$ shift (Yu *et al.*, 2004). However, the mid-infrared spectral pattern between the sorghum and corn were similar. Fig. 3 indicates a heterogeneous distribution of the CH_3 and CH_2 anti-symmetric and symmetric stretch bands. For example, the CH_3 anti-symmetric stretch vibration is highly intensive in the aleurone cell layer, indicating a high concentration (Fig. 3b). Fig. 3 shows that, for the greater number of long-chain CH_2 groups, the corresponding peak intensities are 10–20 times greater than that of CH_3 . This is in agreement with the report by Wetzel & LeVine (2000). It is similar to the findings in Pioneer corn (Yu *et al.*, 2004). Jackson & Mantsch

(2000) indicated that the frequency of the CH_2 stretching absorptions provides a useful probe of lipid bilayer order, lower frequencies being associated with a higher degree of conformational order. It should also be pointed out that protein also contributes to anti-symmetric and symmetric stretching vibrations of the CH_3 (~ 2956 and 2874 cm^{-1}) and CH_2 (~ 2922 and 2852 cm^{-1}) groups. However, compared with lipid it plays a minor role.

Fig. 4 shows the CH_3 to CH_2 anti-symmetric stretch band ratio image in the sorghum seed tissue. The results indicate a high ratio in the sub-aleurone and endosperm region. The pericarp and seed coat regions had relatively the lowest CH_3 to CH_2 anti-symmetric stretch band ratio. The endosperm region was in between [Figs. 4(c) and 4(e)]. When considering the spectral intensity of functional groups and functional group ratios, the degree of freshness of the seeds may affect the imaging. In this case sorghum seed with approximately 90% dry matter content was stored in a cool room at 269 K before section for the synchrotron study.

3.7.2. Imaging the α -helix to β -sheet ratio in protein secondary structure within intact tissue. The protein spectrum has two primary features, the amide I ($\sim 1650 \text{ cm}^{-1}$) and amide II ($\sim 1550 \text{ cm}^{-1}$) bands (Jackson & Mantsch, 1995, 1996, 2000). The vibrational frequency of the amide I band is particularly sensitive to protein secondary structure (Kemp, 1991; Jackson & Mantsch, 1995, 1996, 2000; Miller, 2000; Martin, 2002; Wetzel *et al.*, 2003; Marinkovic *et al.*, 2002; Marinkovic & Chance, 2006) and can be used to predict protein secondary structures

in complex plant systems (Yu, 2006, 2010). The amide II band [predominantly from the N–H bending vibration (60%) coupled to C–N stretching (40%)] is also used to assess the protein conformation (Jackson & Mantsch, 1995, 1996, 2000). However, as it arises from complex vibrations involving multiple functional groups, it is less useful for protein structure prediction than the amide I band (Jackson & Mantsch, 1995, 1996, 2000). Therefore the amide I (1650 cm^{-1}) and amide II (1550 cm^{-1}) bands are characteristics of C=O, C–N and N–H bonds in the protein backbone (Jackson & Mantsch, 1995, 1996, 2000) and are indicators of the area of the sample where protein is present (Yu *et al.*, 2004). Fig. 5(c) shows a molecular

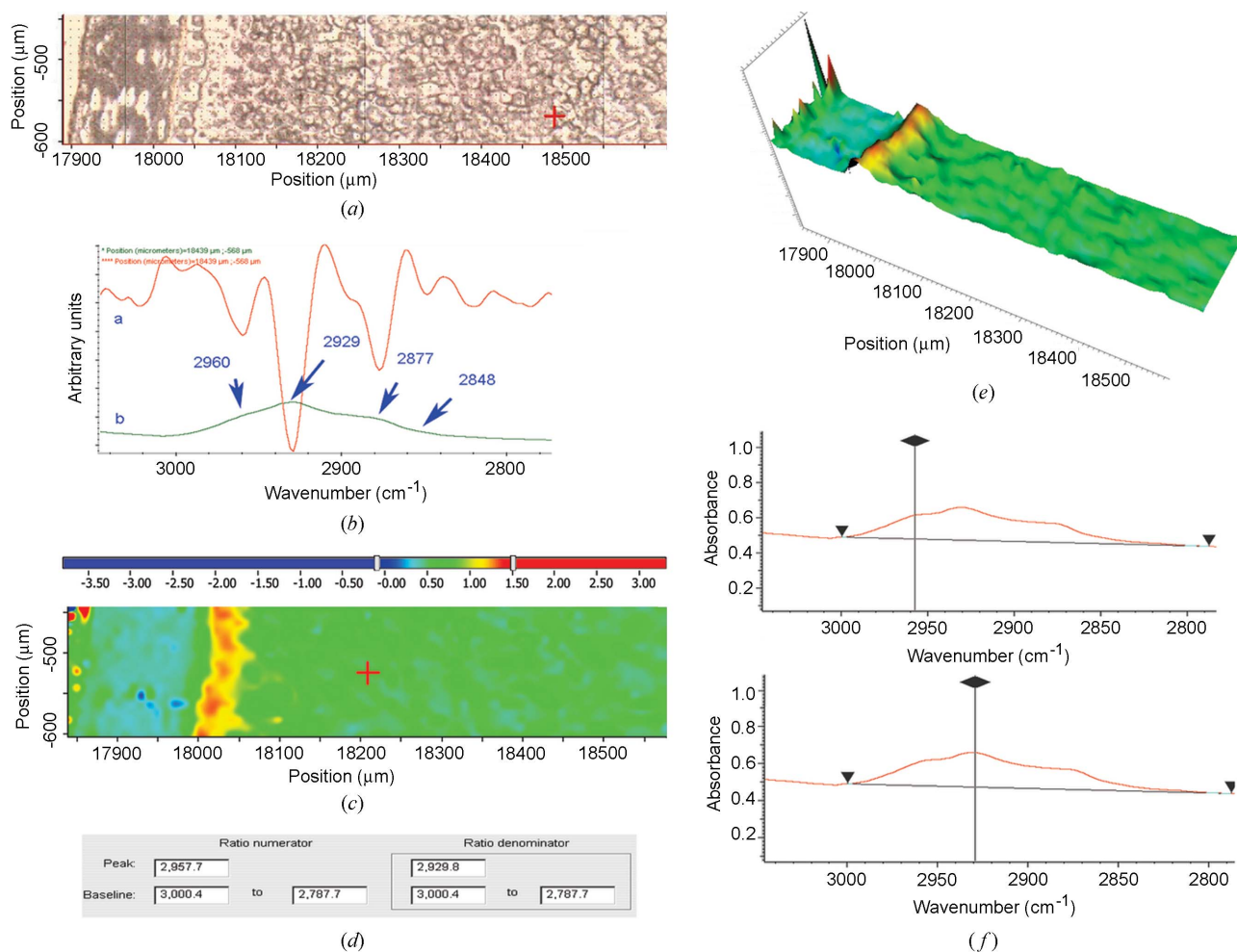


Figure 4 Molecular functional group peak area ratio. Peak height under the CH₃ asymmetric stretch at ~2960 cm⁻¹ divided by the height under the peaks of the CH₂ asymmetric stretch at ~2929 cm⁻¹ at each pixel (pixel size 10 μm × 10 μm), representing the anti-symmetric CH₃ to CH₂ ratio in the sorghum seed tissue. (a) Visible image. (b) Spectra corresponding to the pixel at the cross hair in the visible image. (c) Chemical ratio image: anti-symmetric CH₃ to CH₂ ratio. (d) Region and baseline: anti-symmetric CH₃ and CH₂. (e) Three-dimensional image; peak height ratio of two peaks. (f) Ratio image profile set-up.

functional group peak area ratio image of the height under the protein α -helix (~1657 cm⁻¹) bands divided by the height under the peaks of β -sheet (~1628 cm⁻¹) bands at each pixel (pixel size 10 μm × 10 μm), representing the α -helix to β -sheet-ratio in the sorghum seed tissue. The amide I component peaks were determined by using the second-derivative function. The relative α -helix and β -sheet band assignments are obtained according to various published results. The results showed that the pericarp and seed coat region have no protein associated with them and that protein concentration is high in the aleurone layer and the endosperm areas. The results indicate that the α -helix to β -sheet spectral intensity ratio is unequally distributed, with the strongest ratio in the endosperm region in the sorghum seed tissue [Figs. 5(c) and 5(e)]. The protein α -helix to β -sheet ratio is related to food quality and seed functionality. In a wheat protein secondary structure study, Bonwell *et al.* (2008) reported that one molecular aspect of mature hard wheat protein quality for bread-making is the relative amount of endosperm protein in the α -helix form compared with that in other secondary structure forms

including the β -sheet. Wolkers *et al.* (1998) reported that IMS could detect changes in the protein secondary structure associated with desiccation tolerance in developing maize embryos. It should be noted that the assignments of protein secondary structure for different biological tissues were different. Here it only shows the relative ratio of spectral height intensity of 1657 to 1638 cm⁻¹. For a detailed discussion about protein structure study using synchrotron and peak-modelling techniques, see Jackson & Mantsch (1995, 1996, 2000) and Yu (2005a,b, 2006). There is some potential and questions associated with the modelling techniques (Yu, 2006).

3.7.3. Imaging the protein amide I to total carbohydrate ratio within intact tissue. Fig. 6 shows a molecular functional group ratio image showing the peak area ratio of protein amide I to total carbohydrate and represents the distribution and intensity of the area under the ~1650 cm⁻¹ band divided by the area under the peaks between 1180 and 950 cm⁻¹ at each pixel. The results show that the highest ratio of protein amide I to carbohydrate is in the aleurone cell layer. The pericarp, seed coat and endosperm regions have relatively

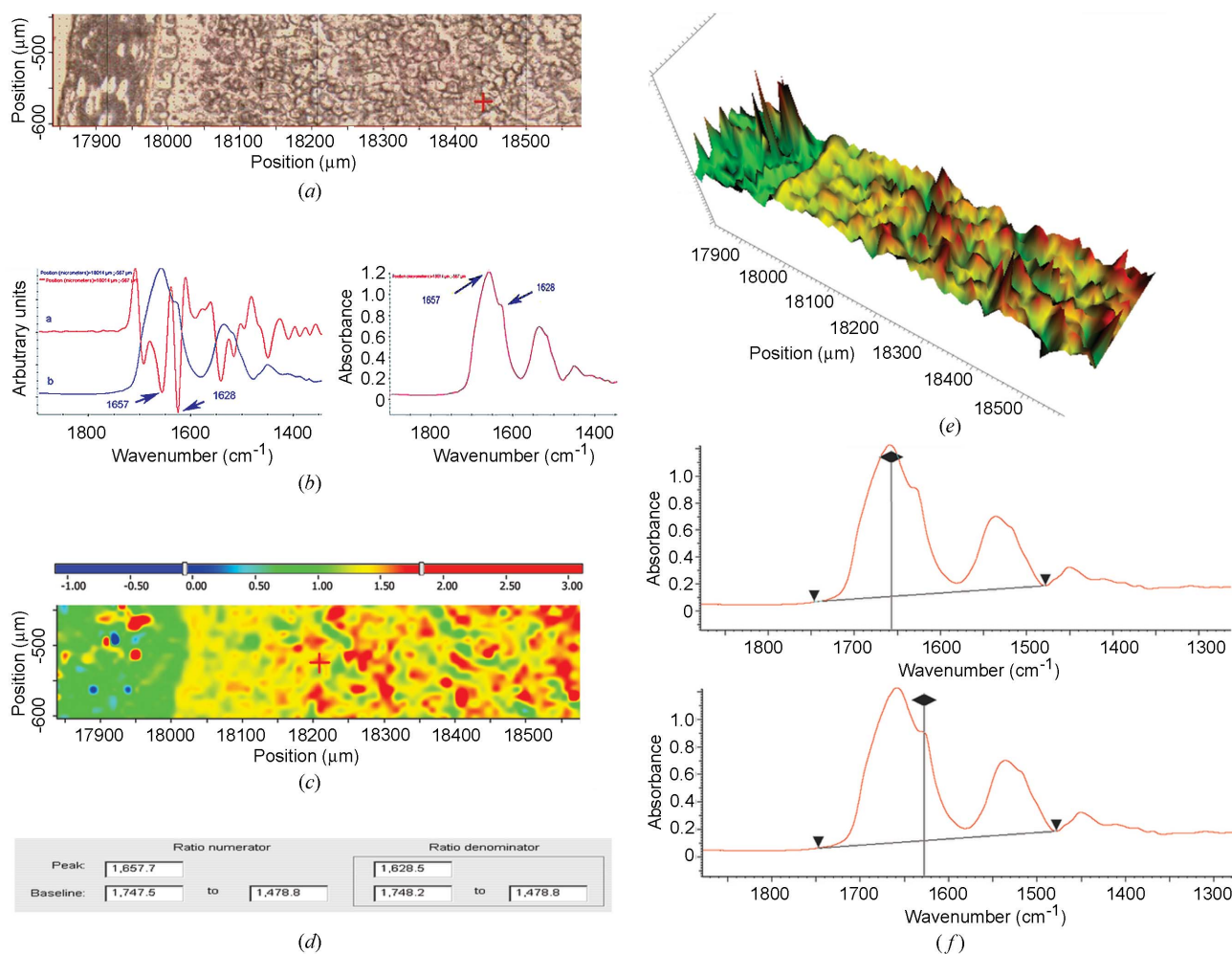


Figure 5

Molecular functional group peak area ratio. Height under the protein α -helix ($\sim 1657 \text{ cm}^{-1}$) bands divided by the height under the peaks of the β -sheet ($\sim 1628 \text{ cm}^{-1}$) bands at each pixel (pixel size $10 \mu\text{m} \times 10 \mu\text{m}$), representing the α -helix to β -sheet ratio in the sorghum seed tissue. (a) Visible image. (b) Spectra corresponding to the pixel at the cross hair in the visible image. (c) Chemical ratio image: α -helix (1657 cm^{-1}) to β -sheet (1628 cm^{-1}). (d) Region and baseline: α -helix (1657 cm^{-1}) to β -sheet (1628 cm^{-1}). (e) Three-dimensional image; peak height ratio of two peaks. (f) Ratio image profile set-up.

lower protein amide I to total carbohydrate ratios (Fig. 4c). Further studies are planned to investigate the potentiality of SR-IMS in monitoring the degradation processing of sorghum tissue in the rumen. It is also possible that the imaging techniques can be used to check the degree of sorghum grain damage (+ = 10% damage, ++ = 20% highly damaged and +++ = 30% severely damaged).

4. Conclusions and implications

In conclusion, the various molecular functional groups which are associated with food and feed quality and functionality of feed-type sorghum could be imaged within intact tissue using the SR-IMS technique. The relative protein secondary structure α -helix to β -sheet ratio, protein amide I to starch granule ratio, and anti-symmetric CH_3 to CH_2 ratio images could also be generated to show the unique molecular spatial distribution, intensity and nutrient make-up/conformation in the sorghum seed tissue. The molecular imaging technique has

high potential and could be used for the development of a specific variety of cereal grain with targeted food and feed quality, and for studying the structural architecture of plants at a cellular level. It could also be used to monitor the degree of grain maturity, grain damage and the effect and fate of organic contaminants and chemical treatment on grains and plants.

This research has been supported by grants from Natural Sciences and Engineering Research Council of Canada (NSERC Individual Discovery Grant), Saskatchewan Agricultural Development Fund and Ministry of Agriculture Strategic Research Chair fund. The National Synchrotron Light Source in Brookhaven National Laboratory (NSLS-BNL, New York, USA) is supported by the US Department of Energy contract DE-AC02-98CH10886. The Case Center for Synchrotron Biosciences, The Center for Proteomics at Case Western Reserve University, was supported by the National Institute for Biomedical Imaging and Bioengineering under NIH grants P41-EB-01979 and P30-EB-009998. We are

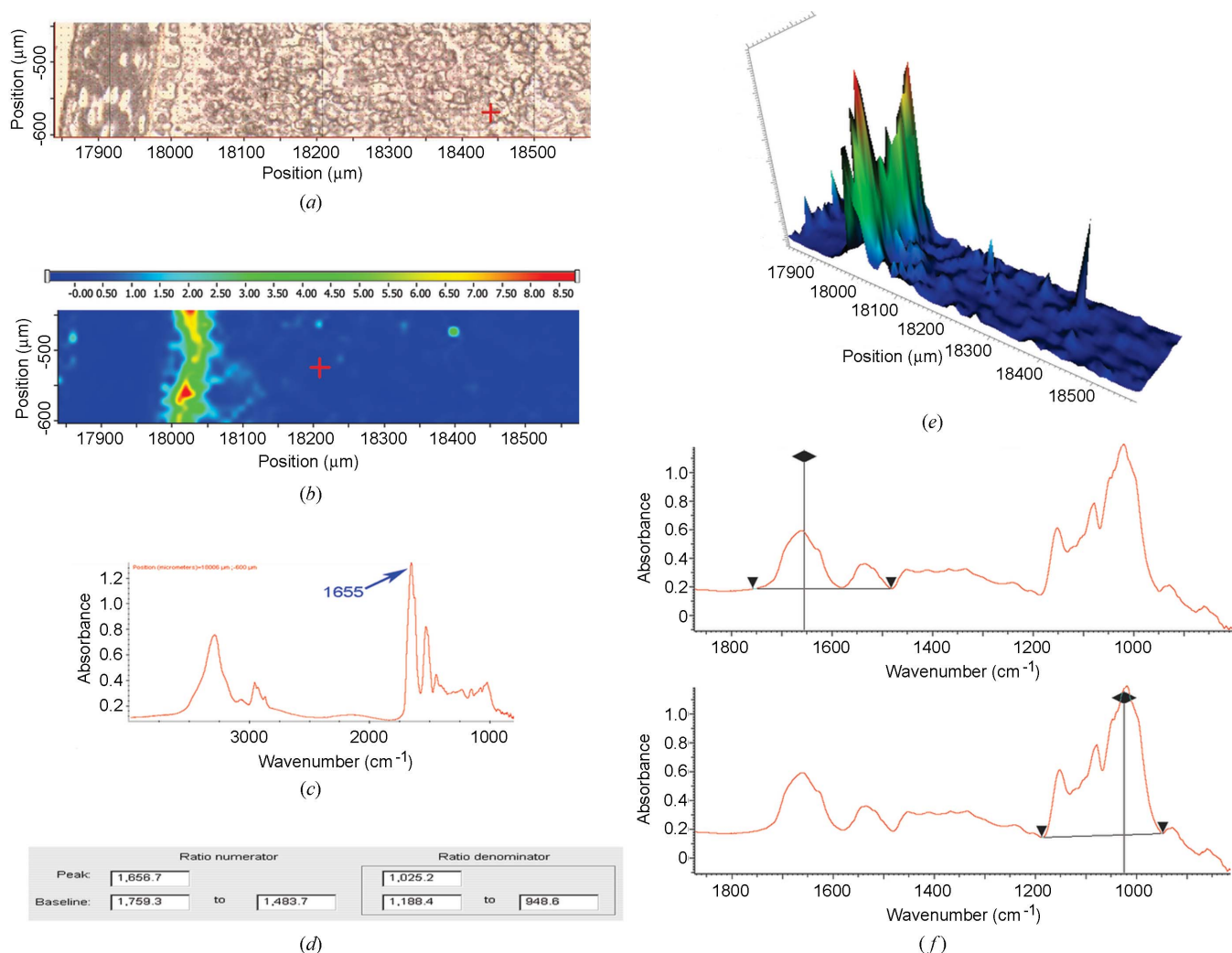


Figure 6 Molecular functional group peak area ratio. Height under the protein amide I (1650 cm^{-1}) bands divided by the height under the peaks between ~ 1180 and 950 cm^{-1} at each pixel (pixel size $10\text{ }\mu\text{m} \times 10\text{ }\mu\text{m}$) representing the protein to total carbohydrate ratio in the sorghum seed tissue. (a) Visible image. (b) Spectra corresponding to the pixel at the cross hair in the visible image. (c) Chemical ratio image: protein to carbohydrate ratio. (d) Region and baseline of protein amide I and II and carbohydrate. (e) Three-dimensional image; peak height ratio of two peaks. (f) Ratio image profile set-up.

grateful to Professor Dr D. Liu (Northeast Agricultural University) for providing the sorghum seeds, Jennifer Bohon (old U2B coordinator), Randy Smith and Lisa Miller (NSLS-BNL) for helpful data collection at the old U2B experimental stations, and Tim May, Luca Quaroni and Ferenc Borondics for helpful data collection in the test runs at station 01B1-1 of the Canadian Light Source, which is supported by various federal and provincial funding agencies in Canada.

References

Bonwell, E. S., Fisher, T. L., Fritz, A. K. & Wetzel, D. L. (2008). *Vib. Spectrosc.* **48**, 76–81.
 Budevskas, B. O. (2002). *Handbook of Vibrational Spectroscopy*, Vol. 5, *Applications of Vibrational Spectroscopy in Life, Pharmaceutical and Natural Sciences*, edited by J. M. Chalmers and P. R. Griffiths, pp. 3720–3732. New York: John Wiley and Sons.
 Burattini, E., Cavagna, M., Dell'Anna, R., Malvezzi Campaggi, F., Monti, F., Rossi, F. & Torriani, S. (2008). *Vib. Spectrosc.* **47**, 139–147.

Chan, K. L., Tay, F. H., Taylor, C. & Kazarian, S. G. (2008). *Appl. Spectrosc.* **62**, 1041–1044.
 CLS (2010). *What is a Synchrotron Anyway?*, <http://www.lightsource.ca/education/whatis.php>.
 Colthup, N. B., Daly, L. H. & Wiberley, S. E. (1990). *Introduction to Infrared and Raman Spectroscopy*, 3rd ed., p 547. Boston: Academic Press.
 Doiron, K. J., Yu, P., Christensen, C. R., Christensen, D. A. & McKinnon, J. J. (2009a). *Spectroscopy*, **23**, 307–322.
 Doiron, K. J., Yu, P., McKinnon, J. J. & Christensen, D. A. (2009b). *J. Dairy Sci.* **92**, 3319–3330.
 Dokken, K. M. (2006). PhD thesis, Kansas State University, USA.
 Dokken, K. M., Davis, L. C., Erickson, L. E., Castro-Diaz, S. & Marinkovic, N. S. (2005). *Microchem. J.* **81**, 86–91.
 Dokken, K. M., Davis, L. C. & Marinkovic, N. S. (2007). *Appl. Spectrosc. Rev.* **40**, 301–326.
 Himmelsbach, D. S., Khalili, S. & Akin, D. E. (1998). *Cell. Mol. Biol.* **44**, 99–108.
 Jackson, M. & Mantsch, H. H. (1995). *Biochem. Mol. Biol.* **30**, 95–120.
 Jackson, M. & Mantsch, H. H. (1996). *Infrared Spectroscopy of Biomolecules*, edited by H. H. Mantsch and D. Chapman, pp. 311–340. New York: Wiley-Liss.

- Jackson, M. & Mantsch, H. H. (2000). *Encyclopedia of Analytical Chemistry*, Vol. 1, edited by R. A. Meyers, pp. 131–156. Chichester: John Wiley and Sons.
- Kemp, W. (1991). *Organic Spectroscopy*, 3rd ed. New York: W. H. Freeman.
- LNF (2003). *Biological Applications of Synchrotron Infrared spectroscopy in Europe (BASIE)*, LNF SIS pubblicazioni LNF-03/004 (NT). Laboratori Nazionali di Frascati, Frascati, Italy.
- McCann, M. C., Chen, L., Roberts, K., Kemsley, E. K., Sene, C., Carpita, N. C., Stacey, N. J. & Wislon, R. H. (1997). *Physiol. Plant.* **100**, 729–738.
- McCann, M. C. & Roberts, K. (1994). *J. Exp. Bot.* **45**, 1683–1691.
- McCann, M. C., Roberts, K., Wilson, R. H., Gidley, M. J., Gibeau, D. M., Kim, J.-B. & Carpita, N. C. (1995). *Can. J. Bot.* **73**, S103–S113.
- Marinkovic, N. S. & Chance, M. R. (2006). *Synchrotron Infrared Microscopy, Encyclopedia of Molecular Cell Biology and Molecular Medicine*, 2nd ed., Vol. 13, edited by R. Meyers, pp. 671–708. New York: Wiley.
- Marinkovic, N. S., Huang, R., Bromberg, P., Sullivan, M., Toomey, J., Miller, L. M., Sperber, E., Moshe, S., Jones, K. W., Chouparova, E., Lappi, S., Franzen, S. & Chance, M. R. (2002). *J. Synchrotron Rad.* **9**, 189–197.
- Martin, M. C. (2002). *Fourier transform infrared spectroscopy*, <http://infrared.als.lbl.gov/>.
- Mathlouthi, M. & Koenig, J. L. (1986). *Adv. Carbohydr. Chem. Biochem.* **44**, 7–89.
- Miller, L. M. (2000). *Synchrotron Rad. News*, **13**, 31–37.
- Miller, L. M. (2009). *Infrared Microspectroscopy and Imaging*, <http://www.nsls.bnl.gov/newsroom/publications/otherpubs/imaging/workshopmiller.pdf>.
- Miller, L. M. & Dumas, P. (2006). *Biochim. Biophys. Acta*, **1758**, 846–857.
- Pietrzak, L. N. & Miller, S. S. (2005). *J. Agric. Food Chem.* **53**, 9304–9311.
- Raab, T. K. & Martin, M. C. (2001). *Planta*, **213**, 881–887.
- Sockalingum, G. D., Bouhedja, W., Pina, P., Allouch, P., Bloy, C. & Manfait, M. (1998). *Cell. Mol. Biol.* **44**, 261–269.
- Stewart, D., McDougall, G. J. & Baty, A. (1995). *J. Agric. Food Chem.* **43**, 1853–1858.
- Vogel, J. P., Raab, T. K., Schiff, C. & Somerville, S. C. (2002). *Plant Cell*, **14**, 2095–2106.
- Wetzel, D. L. (2001). *Proceedings of the International Wheat Quality Conference II*, Manhattan, Kansas, USA, pp. 1–20.
- Wetzel, D. L., Eilert, A. J., Pietrzak, L. N., Miller, S. S. & Sweat, J. A. (1998). *Cell. Mol. Biol.* **44**, 145–167.
- Wetzel, D. L. & LeVine, S. M. (2000). *Infrared and Raman Spectroscopy of Biological Materials*, edited by H. U. Gremlich and B. Yan, pp. 101–142. New York: Marcel Dekkar.
- Wetzel, D. L., Srivarin, P. & Finney, J. R. (2003). *Vib. Spectrosc.* **31**, 109–114.
- Wolkers, W. F., Bochicchio, A., Selvaggi, G. & Hoekstra, F. A. (1998). *Plant Physiol.* **116**, 1169–1177.
- Yu, P. (2004). *Br. J. Nutr.* **92**, 869–885.
- Yu, P. (2005a). *Appl. Spectrosc.* **59**, 1372–1380.
- Yu, P. (2005b). *J. Agric. Food Chem.* **53**, 2872–2880.
- Yu, P. (2006). *Spectroscopy*, **20**, 229–251.
- Yu, P. (2010). *Mol. Nutr. Food Res.* **54**, 1535–1545.
- Yu, P., Block, H., Niu, Z. & Doiron, K. (2007). *J. Synchrotron Rad.* **14**, 382–390.
- Yu, P., McKinnon, J. J., Christensen, C. R. & Christensen, D. A. (2004). *J. Agric. Food Chem.* **52**, 7345–7352.